

Joint Generative Modeling of Scene Graphs and Images via Diffusion Models

Bicheng Xu^{*1,2}Qi Yan^{*1,2}Renjie Liao^{1,2,3}Lele Wang¹Leonid Sigal^{1,2,3}¹University of British Columbia²Vector Institute for AI³Canada CIFAR AI Chair

bichengxu@cs.ubc.ca

{qi.yan, rjliao, lelewang}@ece.ubc.ca

lsigal@cs.ubc.ca

Abstract

In this paper, we present a novel generative task: joint scene graph - image generation. While previous works have explored image generation conditioned on scene graphs or layouts, our task is distinctive and important as it involves generating scene graphs themselves unconditionally from noise, enabling efficient and interpretable control for image generation. Our task is challenging, requiring the generation of plausible scene graphs with heterogeneous attributes for nodes (objects) and edges (relations among objects), including continuous object bounding boxes and discrete object and relation categories. We introduce a novel diffusion model, DiffuseSG, that jointly models the adjacency matrix along with heterogeneous node and edge attributes. We explore various types of encodings for the categorical data, relaxing it into a continuous space. With a graph transformer being the denoiser, DiffuseSG successively denoises the scene graph representation in a continuous space and discretizes the final representation to generate the clean scene graph. Additionally, we introduce an IoU regularization to enhance the empirical performance. Our model significantly outperforms existing methods in scene graph generation on the Visual Genome and COCO-Stuff datasets, both on standard and newly introduced metrics that better capture the problem complexity. Moreover, we demonstrate the additional benefits of our model in two downstream applications: 1) excelling in a series of scene graph completion tasks, and 2) improving scene graph detection models by using extra training samples generated from DiffuseSG.

1. Introduction

Scene graph is a graph-based representation that captures semantics of the visual scene, where nodes correspond to the objects (including their identity/labels and spatial locations) and directed edges correspond to the spatial and functional relations between pairs of objects. Scene graphs have been widely adopted in a variety of high-level tasks,

*Equal contribution

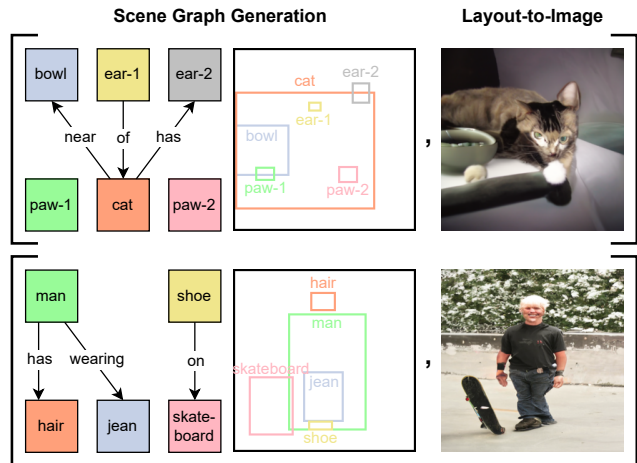


Figure 1. **Joint Scene Graph and Image Modeling.** We model the joint distribution of scene graph - image pairs via two steps: first training our proposed DiffuseSG model to produce scene graphs and then utilizing a pretrained layout-to-image model [72] to generate images. Results shown are sampled from models trained on the Visual Genome dataset.

including image captioning [65, 75] and visual question answering [8, 48]. Various models [3, 21, 24, 32, 71] have been proposed to predict scene graphs from images. Such models require supervised training with image-scene graph pairs, which is costly to annotate.

Motivated by this and the recent successes of generative models, in this paper, we introduce the problem of joint generative modeling of scene graphs and corresponding images. The benefits of such generative model would be multifaceted. First, it can be used to generate *synthetic* training data to augment training of discriminative scene graph prediction approaches discussed above. Second, it can serve as a generative scene prior which can be tasked with visualizing likely configurations of objects in the scene conditioned on partial observations. For example, where is the likely position of the chair given placement of the table and sofa. Third, it can be used for controlled image generation, by allowing users to automatically sample and edit scene graphs

and, conditioned on them, generate corresponding images.

Generative models, diffusion models [16, 55, 56] in particular, have been shown to excel at modeling complex distributions, generating realistic high-resolution images [46, 51, 53, 54] and graphs [22, 62, 64]. However, the proposed task is uniquely challenging in that it requires joint generation of an image and a corresponding graph representation. Therefore, to simplify the task, we factorize the joint distribution as a product of a *scene graph prior* and a conditional distribution of images given a scene graph. The conditional distribution has been widely studied in the form of *layout-to-image generation* [57, 58, 70, 72] – a task of generating images based on spatial layouts that can be constructed from scene graphs¹. Therefore, in this paper we mainly focus on modeling the first term, *i.e.*, building a generative scene graph model. This task in itself is challenging as it requires generation of graphs with heterogeneous attributes, *e.g.*, real-valued node attributes like object bounding boxes and categorical edge attributes like relation types.

To solve the newly proposed task, we propose DiffuseSG which is a diffusion-based generative model capable of generating plausible scene graphs. To deal with heterogeneous attributes, we explore various encodings of categorical node/edge representations to relax them into a continuous space. We also design a graph transformer architecture that successively denoises the continuous graph representation which in the end produces clean scene graph samples via simple discretization. Lastly, we introduce an intersection-over-union (IoU)-based training loss to better capture the distribution of bounding box locations and sizes.

In summary, our contributions are as follows. (1) We propose a novel joint scene graph - image generation task. (2) We propose a diffusion-based model, named DiffuseSG, which jointly models the adjacency matrix, node attributes like object classes and bounding boxes, and edge attributes like object relations. (3) We show that our model significantly outperforms existing general-purpose graph generative models on both standard and newly introduced metrics that better measure the similarity between observed and generated scene graphs. (4) We show that our model performs well on various scene graph completion tasks using diffusion guidance. Moreover, paired with a layout-to-image generative model, our model generates scene graph - image pairs which serve as extra training data for the downstream scene graph prediction task. The observed performance improvement highlights the practical significance of our new task in real-world applications.

2. Related Work

Diffusion Models. Diffusion models achieve great success in a variety of generation tasks nowadays, ranging

¹Though, notably, in the process, edge information is often not utilized.

from image generation [4, 27, 31, 39, 69], video generation [11, 14, 47, 66], text generation [12, 38, 40], and simple graph generation [22, 62, 64], *e.g.*, on molecule datasets [19, 49], which usually have less than 10 node types and less than 5 edge types. These models contain two key processes: a forward process, which typically involves adding Gaussian noise to clean data, and a reverse process that is often implemented using architectures such as U-Net [52] or Transformer [61]. Since the scene graph is fundamentally a graph structure, our proposed scene graph generation model is conceptually similar to the ones for simple graph generation. However, our model goes beyond merely generating the graph structure of node (object) and edge (relation) labels. It also generates the object locations, in the form of bounding boxes. Also, our scene graph data is more complex than the molecule data in terms of the number of node and edge types, *e.g.*, the Visual Genome dataset [29] contains 150 node and 50 edge types. This diversity necessitates a reevaluation of many design choices traditionally made in graph generation models.

Layout Generation. Layout generation focuses on creating image layouts, which comprise object labels and their corresponding bounding box locations. In contrast, our proposed scene graph generation goes a step further by also generating the relationships among these objects. Existing layout generation models typically take the form of VAE [1, 25, 33], GAN [35], Transformer or BERT type language models [13, 20, 28], or diffusion models [6, 17, 18, 34, 68]. These layout generation models usually work on graphical layout generation problems, *e.g.*, designing layouts for mobile applications [9, 41], documents [74], or magazines [73]. The object bounding boxes of these layouts are expected to be well-aligned and not overlapping with each other. Thus, the layout generation models are usually measured on the alignment and intersection area of the generated bounding boxes. However, the object bounding boxes in our scene graphs are naturally not aligned and usually occlusions occur. Therefore, we replace the evaluation metrics used in the layout generation literature with new ones that better capture characteristics of scene graphs.

3. Joint Scene Graph - Image Pair Modeling

We propose to model the joint distribution of scene graphs and their corresponding images via two steps. Denote the scene graph by \mathcal{S} and the image by \mathcal{I} ². First, we build a scene graph generation model to learn $p(\mathcal{S})$, *i.e.*, the underlying data distribution of scene graphs. Second, we employ a conditional image generation model (*e.g.*, a layout-to-image model) to capture $p(\mathcal{I}|\mathcal{S})$, the conditional image distribution. The joint distribution of scene graph and image pairs can be represented as $p(\mathcal{S}, \mathcal{I}) = p(\mathcal{S})p(\mathcal{I}|\mathcal{S})$, from

²In what follows, we use \mathbf{I}_d for identity matrix and \mathbf{I} for image data.

which one can easily draw samples in a two-step manner. Our proposed scene graph generation task is formally defined as follows.

Scene Graph Generation Task. A scene graph \mathcal{S} , consisting of n nodes, can be described using node and edge tensors, denoted as (\mathbf{V}, \mathbf{E}) . We denote the space of node features by \mathcal{V} and the space of edge features by \mathcal{E} , and the space of scene graphs by $\mathcal{S} = \mathcal{V} \times \mathcal{E}$. The node tensor $\mathbf{V} = [\mathbf{v}_1; \mathbf{v}_2; \dots; \mathbf{v}_n] \in \mathbb{R}^{n \times d_v}$, captures the node labels and their bounding box locations, where d_v represents the dimension of the node feature. Each node feature $\mathbf{v}_i = [c_i, \mathbf{b}_i]$ combines a discrete node label, $c_i \in \{1, 2, \dots, Z_v\}$, with a normalized bounding box position, $\mathbf{b}_i \in [0, 1]^4$. The bounding box \mathbf{b}_i is represented by (center _{x} , center _{y} , width, height) and normalized w.r.t. the image canvas size. The edge tensor $\mathbf{E} \in \mathbb{R}^{n \times n}$, details the directed edge relationships among the nodes. Each edge entry $e_{i,j}$ corresponds to a discrete relation label, $e_{i,j} \in \{0, \dots, Z_e\}$, clarifying the connections between nodes. The symbols Z_v and Z_e represent the total numbers of semantic object categories and relation categories of interest, respectively. Notably, $e_{i,j} = 0$ indicates the absence of a relation between nodes i and j .

In what follows, we present our DiffuseSG model, specifically designed for the task of scene graph generation. DiffuseSG is a continuous diffusion model, whose training and sampling utilize the stochastic differential equation (SDE) formulation. We begin by providing some background on the SDE-based diffusion modeling, followed by an in-depth explanation of the DiffuseSG model.

3.1. Diffusion Model Basics

Preliminaries. Diffusion models [16, 56] learn a probabilistic distribution $p_\theta(\mathbf{x})$ ³ through matching the score functions of the Gaussian noise perturbed data distribution $\nabla_{\mathbf{x}} \log p_\sigma(\mathbf{x})$ at various noise levels $\sigma \in \{\sigma_i\}_{i=1}^T$. Following [26, 56], we use the SDE based diffusion models for training and sampling, which comes with a continuous time $t \in [0, T]$ specified by the following dynamics:

$$d\mathbf{x}_+ = f(\mathbf{x}, t)dt + g(t)d\mathbf{w}, \quad (1)$$

$$d\mathbf{x}_- = [f(\mathbf{x}, t)dt - g(t)^2 \nabla_{\mathbf{x}} \log p_t(\mathbf{x})]dt + g(t)d\mathbf{w}, \quad (2)$$

where Eq. (1) and Eq. (2) denote forward and reverse SDEs, $f(\mathbf{x}, t)$ and $g(t)$ are the drift and diffusion coefficients, and \mathbf{w} is the standard Wiener process. The SDEs govern how the probabilistic distribution $p_t(\mathbf{x})$ evolves w.r.t. time t . Specifically, $p_0(\mathbf{x})$ is the data distribution, from which we observed a set of i.i.d. samples $\mathcal{X} = \{\mathbf{x}_i\}_{i=1}^m$. $p_T(\mathbf{x})$ models a tractable prior distribution (i.e., Gaussian), from which we can draw samples efficiently. In

³We use symbols $\mathbf{x}, \tilde{\mathbf{x}}$ in this section to introduce preliminaries of diffusion model in general, regardless of the type of data being modeled.

our formulation, we choose linear noise schedule $\sigma(t) = t$, and let $f(\mathbf{x}, t) = \mathbf{0}$ and $g(t) = \sqrt{2\dot{\sigma}(t)\sigma(t)}$. The SDEs solution yields that p_t in Eq. (2) becomes $p_\sigma(\mathbf{x}) = p_t(\mathbf{x}) = \frac{1}{m} \sum_{i=1}^m \mathcal{N}(\mathbf{x}; \mathbf{x}_i, \sigma^2 \mathbf{I}_d)$, $\mathbf{x}_i \in \mathcal{X}$. Let $p_{\mathcal{X}}(\mathbf{x}) = \frac{1}{m} \sum_{i=1}^m \delta(\mathbf{x} - \mathbf{x}_i)$ be the Dirac delta distribution for \mathcal{X} . We can rewrite p_σ as $p_\sigma(\tilde{\mathbf{x}}) = \int p_{\mathcal{X}}(\mathbf{x}) p_\sigma(\tilde{\mathbf{x}}|\mathbf{x}) d\mathbf{x}$ with a Gaussian perturbation kernel $p_\sigma(\tilde{\mathbf{x}}|\mathbf{x}) = \mathcal{N}(\tilde{\mathbf{x}}; \mathbf{x}, \sigma^2 \mathbf{I}_d)$.

Training. We train a neural network to learn the score function of p_σ (i.e., $\nabla_{\tilde{\mathbf{x}}} \log p_\sigma(\tilde{\mathbf{x}})$). Following [26], we reparameterize the score function by denoising function $D(\tilde{\mathbf{x}}, \sigma)$ which maps the noise-corrupted data $\tilde{\mathbf{x}}$ back to the clean data \mathbf{x} . They are connected by Tweedie’s formula [10], $\nabla_{\tilde{\mathbf{x}}} \log p_\sigma(\tilde{\mathbf{x}}) = (D(\tilde{\mathbf{x}}, \sigma) - \tilde{\mathbf{x}})/\sigma^2$. In practice, we train a denoiser $D_\theta(\tilde{\mathbf{x}}, \sigma)$ to implicitly capture the score function. Given a specified distribution over the noise level, denoted as $p(\sigma)$, which also corresponds to the distribution of forward time t since $\sigma(t) = t$, the overall training objective can be formulated as follows:

$$\mathbb{E}_{p(\sigma)p_{\mathcal{X}}(\mathbf{x})p_\sigma(\tilde{\mathbf{x}}|\mathbf{x})} [\|D_\theta(\tilde{\mathbf{x}}, \sigma) - \mathbf{x}\|_2^2]. \quad (3)$$

Sampling. To draw samples using the learned diffusion models, we discretize the reverse-time SDE in Eq. (2) and conduct numerical integration, which gradually transitions samples from prior distribution p_T to data distribution p_0 . We choose a set of discrete time steps $\{t_i\}_{i=1}^T$, at which the score function is evaluated using the trained model for numerical reverse-SDE solution. We employ a second-order solver based on Heun’s method [26, 59].

3.2. DiffuseSG for Scene Graph Generation

We propose to model the scene graph distribution $p(\mathcal{S})$ with a continuous state diffusion model. Our model captures the distribution of scene graph topology along with node and edge attributes simultaneously.

Denoising Objective. During training, we draw noisy scene graph samples from the perturbed distribution $p_\sigma(\tilde{\mathcal{S}}) = \int p_{\mathcal{S}}(\mathcal{S}) p_\sigma(\tilde{\mathcal{S}}|\mathcal{S}) d\mathcal{S}$ and train a denoiser $D_\theta(\tilde{\mathcal{S}}, \sigma)$ to output the associated noise-free samples \mathcal{S} . We relax node and edge label distributions to continuous space, enabling SDE based diffusion modeling with smooth Gaussian noise on all attributes. Various methods for encoding discrete labels will be introduced later. Specifically, $\tilde{\mathcal{S}} = (\tilde{\mathbf{V}}, \tilde{\mathbf{E}})$ denotes the noisy scene graph and $p_{\mathcal{S}}(\mathcal{S}) = \frac{1}{m} \sum_{i=1}^m \delta(\mathcal{S} - \mathcal{S}_i)$ is the Dirac delta distribution based on training data $\{\mathcal{S}_i\}_{i=1}^m$. We implement the scene graph Gaussian perturbation kernel $p_\sigma(\tilde{\mathcal{S}}|\mathcal{S})$ by independently injecting noise to node and edge attributes, i.e., $p_\sigma(\tilde{\mathcal{S}}) = \int p_{\mathcal{S}}(\mathcal{S}) p_\sigma(\tilde{\mathbf{V}}|\mathbf{V}) p_\sigma(\tilde{\mathbf{E}}|\mathbf{E}) d\mathcal{S}$. The decomposed kernels are both simple Gaussians: $p_\sigma(\tilde{\mathbf{V}}|\mathbf{V}) = \mathcal{N}(\tilde{\mathbf{V}}; \mathbf{V}, \sigma^2 \mathbf{I}_d)$, $p_\sigma(\tilde{\mathbf{E}}|\mathbf{E}) = \mathcal{N}(\tilde{\mathbf{E}}; \mathbf{E}, \sigma^2 \mathbf{I}_d)$. Further, we design a denoising network D_θ with two prediction heads D_θ^V and D_θ^E ded-

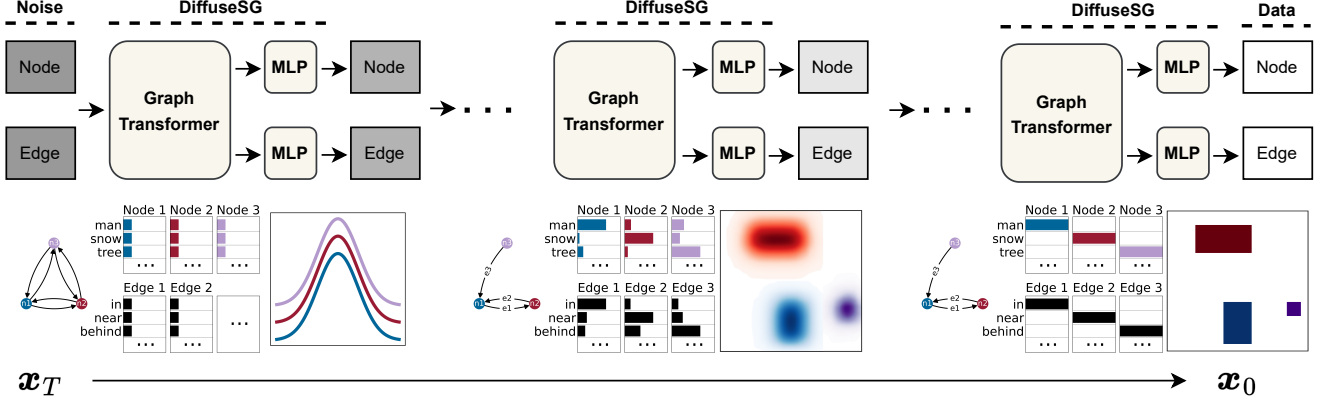


Figure 2. **Sampling Process Illustration.** Starting from Gaussian noise, our DiffuseSG model gradually generates scene graphs with node and edge attributes. Our diffusion process is defined in the continuous space and we conduct discretization to obtain categorical data.

icated to node and edge attributes respectively (detailed below). Our scene graph denoising loss now becomes:

$$\mathcal{L}_d = \mathbb{E}_{p(\sigma)p_S(S)p_\sigma(\tilde{S}|S)} [\|D_\theta^V(\tilde{S}, \sigma) - V\|_2^2 + \|D_\theta^E(\tilde{S}, \sigma) - E\|_F^2]. \quad (4)$$

Network Design. To effectively capture the complex distribution of scene graphs, we develop a transformer architecture, termed *graph transformer*, as the denoiser D_θ . Given a noisy scene graph $\tilde{S} = (\tilde{V}, \tilde{E})$ as input, we construct triplet representations (*i.e.*, generalized edge representations) by concatenating the subject node, object node, and relation information $\tilde{Q}[i, j] = [\tilde{v}_i, \tilde{v}_j, \tilde{e}_{i,j}], \forall i, j \in [n]$. The denoising task is essentially node and edge regression in continuous space, trained with stochasticity. For expressive graph representation learning in this context, we consider message passing among all $O(n^2)$ triplets as suggested in [44, 45]. Here, each triplet becomes a unit of message passing. However, a naive triplet-to-triplet message passing implementation is space-consuming ($O(n^4)$ messages). Inspired by [42], we employ an approximate triplet-to-triplet message passing using shifted-window attention layers with a window size M , which reduces the space complexity to $O(n^2 M^2)$. When window-partitioning is repeated adequately (*e.g.*, at least $O(n/M)$ times), all triplet-to-triplet interactions can be effectively approximated. We tokenize the noisy triplets using a linear layer on each entry in \tilde{Q} , resulting in $n \times n$ triplet tokens of dimension d_t , represented as $\tilde{Q}_d \in \mathbb{R}^{n \times n \times d_t}$. Our graph transformer then employs repeated shifted-window attention and downsampling/upsampling layers to update the dense triplet-token representations, for predicting the noise-free node and edge attributes. To generate node and edge attribute predictions of distinct shapes, we employ two MLPs as readout layers to construct node and edge denoisers D_θ^V and D_θ^E respectively. These components share identical intermediate feature maps and have the same parameters up to the final prediction heads.

Encoding Discrete Data. We adapt the categorical node label c_i and edge label $e_{i,j}$ into a continuous space to facilitate the SDE-based diffusion modeling. The relaxed representations of these discrete data are denoted as $c'_i \in \mathbb{R}^{d_c}$ for node labels and $e'_{i,j} \in \mathbb{R}^{d_e}$ for edge labels. Three distinct encoding methods are explored: (1) Scalar: both node and edge labels are expressed as scalar values, with $d_c = d_e = 1$. (2) Binary-Bit Encoding: the discrete type indices of node and edge labels are converted into their binary format, represented as a sequence of 0s and 1s. Here, $d_c = \lceil \log_2(Z_v) \rceil$ and $d_e = \lceil \log_2(Z_e + 1) \rceil$. (3) One-Hot Encoding: the scalar labels are transformed into their one-hot representations, resulting in $d_c = Z_v$ and $d_e = Z_e + 1$. The impact of these different encoding methods is further analyzed and compared in Sec. 4.3. During the sampling process, we discretize the continuous-valued representations of node and edge types, *e.g.*, through thresholding for the binary-bit encoding. Detailed explanations of these encodings are in the Supplemental. Note that the bounding box positions b_i are naturally continuous and there is no need for special encoding. The sampling pipeline is illustrated in Fig. 2.

Additional Bounding Box IoU Loss. To enhance bounding box generation quality, we integrate an intersection-over-union (IoU) based loss, \mathcal{L}_{iou} , into the denoising objective. This IoU loss aims to align the denoised bounding box $\hat{B} \in \mathbb{R}^{n \times 4}$ (a partial output of D_θ^V) closely with the ground-truth $B \in \mathbb{R}^{n \times 4}$. The IoU loss is formulated as:

$$\mathcal{L}_{iou} = 1 - \frac{1}{n} \sum_{i=1}^n \text{GIoU}(\hat{B}_i, B_i), \quad (5)$$

where GIoU is the generalized IoU, proposed in [50], of the corresponding boxes. The final training loss then becomes:

$$\mathcal{L} = \mathcal{L}_d + \lambda \mathcal{L}_{iou}, \quad (6)$$

where λ is a hyper-parameter that adjusts the balance

between these two loss components; note, \mathcal{L}_d is given in Eq. (4). We use $\lambda = 1$ in our experiments.

4. Experiments

We conduct all experiments on the VG [29] and COCO-Stuff [5] datasets. The network architecture and implementation details of DiffuseSG are detailed in the Supplemental.

4.1. Datasets

Visual Genome (VG). We use the same pre-processing procedure and train/val splits as previous scene graph detection works [37, 60, 63, 67], but only the scene graph annotations are used. This pre-processed dataset contains 57,723 training and 5,000 validation scene graphs with 150 object and 50 semantic relation categories. For each scene graph, we ensure that there will be only one edge label if there exists a directed edge (relation) between two nodes (objects). Each scene graph has node numbers between 2 and 62, with an average of 5.15 relations per instance.

COCO-Stuff. COCO-Stuff contains 171 object types (including 80 thing and 91 stuff categories). It comes with object label and bounding box annotations, but no relation labels. Following [23], we manually assign a relation label between two bounding boxes based on their relative positions, with a relation set of 6 labels: left of, right of, above, below, inside, and surrounding. Same as in [28], we remove small bounding boxes ($\leq 2\%$ image area) and instances tagged as “iscrowd”, resulting in 118,262 training and 4,999 validation scene graphs. Each scene graph is a fully-connected graph without self-loop, with node numbers between 1 and 33.

4.2. Evaluation Metrics and Baselines

We use maximum mean discrepancy (MMD), triplet total variation difference (TV), and our proposed novel object detection based F1 scores to measure the model performance on the scene graph generation task.

MMD. MMD is used to measure the similarities between generated scene graphs and ground-truth ones on the node degree, node label, and edge label aspects. Gaussian kernel is used for the MMD calculation.

Triplet TV. As the $\langle \text{subject}, \text{relation}, \text{object} \rangle$ triplet lies in a very high dimension (the cross product of potential subject, relation, and object types), it is computationally infeasible to calculate the triplet MMD. As a compromise, we use TV to measure the marginal distribution difference between the generated triplet set and the ground-truth one.

Detection based F1 Scores. We propose a set of novel object detection based F1 scores to evaluate the generated bounding box layout quality (including both the location

and node label). Specifically, for a generated layout, we calculate a F1 score between this generated layout and every ground-truth layout, and take the maximum one as the final score. Given a pair of generated and ground-truth layouts, the F1 score is calculated as $F1 = \frac{1}{|N|} \sum_{c \in N} (w_c \cdot F1_c)$, where N is the node category set, $F1_c$ is the F1 score for a node category c , and w_c is its weighting coefficient with $\frac{\sum_c w_c}{|N|} = 1$. Calculating $F1_c$ needs to decide whether two bounding boxes match or not. We use 10 different bounding box IoU thresholds ranging from 0.05 to 0.5 with a step size of 0.05 to decide the bounding box match. That is, $F1_c = \frac{1}{10} \sum_{iou \in [0.05:0.05:0.5]} F1(iou|c)$, where $F1(iou|c)$ means a F1 score between two layouts given a specific node category c and a IoU threshold iou . We calculate 4 different types of F1 scores: (1) F1-Vanilla (F1-V), where w_c is set to 1 for every node category; (2) F1-Area (F1-A), where w_c is set according to the average bounding box area in the validation set for the node category c . (3) F1-Frequency (F1-F): where w_c is set according to the frequency of the node category c in the validation set; (4) F1-BBox Only (F1-BO): where the F1 calculation is purely based on the bounding box locations, that is, we treat all bounding boxes as having a single node category ($|N| = 1$ and $w_c = 1$). The motivation of having F1-Area and F1-Frequency is that we want some metrics to be slightly biased to those salient objects (appearing either in a large size in general or more frequently).

Baselines. We consider the following four baselines. (1) BLT [28], which is a transformer based layout generation model where only node labels and bounding boxes are generated. The bounding box locations are represented as discrete tokens. (2) LayoutDM [18], which is a discrete state-space diffusion layout generation model. The bounding box locations are also discretized. (3) D3PM [2], which is a discrete denoising diffusion probabilistic framework designed for discrete data generation. We take its image generation model for the scene graph generation task; details are in the Supplemental. This model only generates node and edge labels. (4) DiGress [62], which is a discrete denoising diffusion model for generating graphs with categorical node and edge labels. We add an additional input of discrete bounding box representation, same as the one used in LayoutDM, to incorporate bounding box generation. For all the baselines, we train them from scratch using the authors’ released code, with slight adaptation to the datasets.

4.3. Scene Graph Generation Results

Our DiffuseSG is trained with Eq. (6) and uses the binary-bit input representation. We also conduct experiments with different input representations (binary-bit, scalar, one-hot) without the IoU loss Eq. (5): DiffuseSG⁻ (bit), DiffuseSG⁻ (scalar), and DiffuseSG⁻ (one hot). For all our models and

Visual Genome (VG)									
Method	N-MMD↓	F1-V↑	F1-A↑	F1-F↑	F1-BO↑	D-MMD↓	E-MMD↓	T-TV (val)↓	TV (train)↓
BLT [28]	2.70e-2	0.181	<u>0.300</u>	0.376	0.708	-	-	-	-
LayoutDM [18]	3.02e-2	0.136	0.279	0.272	<u>0.738</u>	-	-	-	-
D3PM [2]	7.69e-3	-	-	-	-	2.00e-2	<u>2.00e-2</u>	0.816	0.772
DiGress [62]	7.94e-3	0.157	0.263	0.282	0.732	4.45e-3	8.02e-3	0.718	0.706
DiffuseSG	6.64e-3	0.184	0.308	<u>0.292</u>	0.747	2.97e-3	3.46e-2	0.702	0.685
DiffuseSG ⁻ (bit)	<u>6.57e-3</u>	0.173	0.285	0.283	0.736	<u>2.99e-3</u>	3.40e-2	<u>0.709</u>	<u>0.692</u>
DiffuseSG ⁻ (scalar)	8.65e-3	0.168	0.267	0.276	0.712	5.23e-3	4.77e-2	0.729	0.713
DiffuseSG ⁻ (one hot)	3.05e-3	0.142	0.249	0.253	0.689	8.46e-3	5.77e-2	0.795	0.751

COCO-Stuff									
Method	N-MMD↓	F1-V↑	F1-A↑	F1-F↑	F1-BO↑	D-MMD↓	E-MMD↓	T-TV (val)↓	T-TV (train)↓
BLT [28]	1.09e-1	0.322	0.389	0.526	0.807	-	-	-	-
LayoutDM [18]	3.12e-2	0.229	0.382	0.576	0.815	-	-	-	-
D3PM [2]	3.45e-4	-	-	-	-	0	1.28e-4	0.341	0.305
DiGress [62]	1.06e-3	0.342	0.387	0.570	0.782	0	4.44e-3	0.515	0.398
DiffuseSG	<u>5.53e-4</u>	<u>0.421</u>	0.485	0.637	0.830	0	7.25e-5	0.270	0.219
DiffuseSG ⁻ (bit)	5.63e-4	0.422	<u>0.481</u>	<u>0.634</u>	<u>0.821</u>	0	<u>7.94e-5</u>	<u>0.272</u>	<u>0.225</u>
DiffuseSG ⁻ (scalar)	8.72e-4	0.380	0.432	0.605	0.788	0	4.65e-4	0.312	0.282
DiffuseSG ⁻ (one hot)	2.35e-3	0.365	0.372	0.553	0.762	0	1.82e-3	0.439	0.332

Table 1. **Scene Graph Generation Results** on the Visual Genome and COCO-Stuff validation sets. In each column, the best value is **bolded**, and the second best value is underlined. N-MMD, D-MMD, and E-MMD are the MMD values calculated based on node label distribution, node degree distribution, and edge label distribution respectively. T-TV (val) / (train) is the triplet TV calculated against validation / training triplet statistics. The training set has a larger set of triplets than the validation, giving a more comprehensive evaluation.

baselines, we consistently randomly sample a fixed set of 1,000 training samples to do model selection.

Tab. 1 shows the quantitative results. For each model, we generate 3 sets of layout or scene graph samples via giving the node numbers in the respective validation set. Reported results are the averaged results over the 3 sample sets. From the table, we can see that our DiffuseSG achieves the best results on most evaluation metrics. Comparing to the baselines, on VG, DiffuseSG only performs worse than BLT on F1-F and worse than D3PM and DiGress on E-MMD. On COCO-Stuff, DiffuseSG is only worse than D3PM on N-MMD, but the gap is very small, in a degree of 10^{-4} . Since all the scene graphs in COCO-Stuff are fully-connected, all the scene graph generation models learn the pattern, resulting in a D-MMD with all 0 values. Comparing DiffuseSG with DiffuseSG⁻ (bit) on the F1 scores, we can see the effectiveness of our proposed IoU loss. Because it measures area instead of just distances in individual dimensions, resulting in a better bounding box generation quality. Comparing among the three different input encoding methods on DiffuseSG⁻, the binary-bit representation works the best on both datasets. Some qualitative results for DiffuseSG are shown in Fig. 3. As can be seen, the generated scene graphs are reasonable. On VG, DiffuseSG learns the sparsity of the semantic edges. While on COCO-Stuff, DiffuseSG captures the fully-connected graph pattern.

4.4. Scene Graph Completion

Our proposed DiffuseSG is versatile, besides doing the pure scene graph generation, it can also achieve a variety of scene graph completion tasks. We mainly follow [43] for all the completions. All completion tasks are conducted on VG.

Single Node Label Completion. In this setting, we randomly masked out one node label per scene graph in the validation set. For each scene graph, we keep all the bounding box locations and edge labels, and let the model to complete one node label given the remaining ones. The node whose label is masked out has degree (sum of in-degree and out-degree) at least 1. This random masking is only done once, that is, it is fixed when evaluating the models. For each validation scene graph, we conduct the completion 200 times, and report the Hit Rate @ K (**HR@K**) and mean accuracy (**mA**) values. For each masked scene graph, to calculate the HR@K, we first build a node label histogram from the 200 completions over the 150 object categories, and then keep the predictions from the K most frequently predicted node categories. We assign a score of 1 if there is one prediction from the kept prediction set matches the ground-truth node label, and a score of 0 otherwise. If there are multiple categories on the boundary when selecting the top K predicted categories, we randomly select some of them to

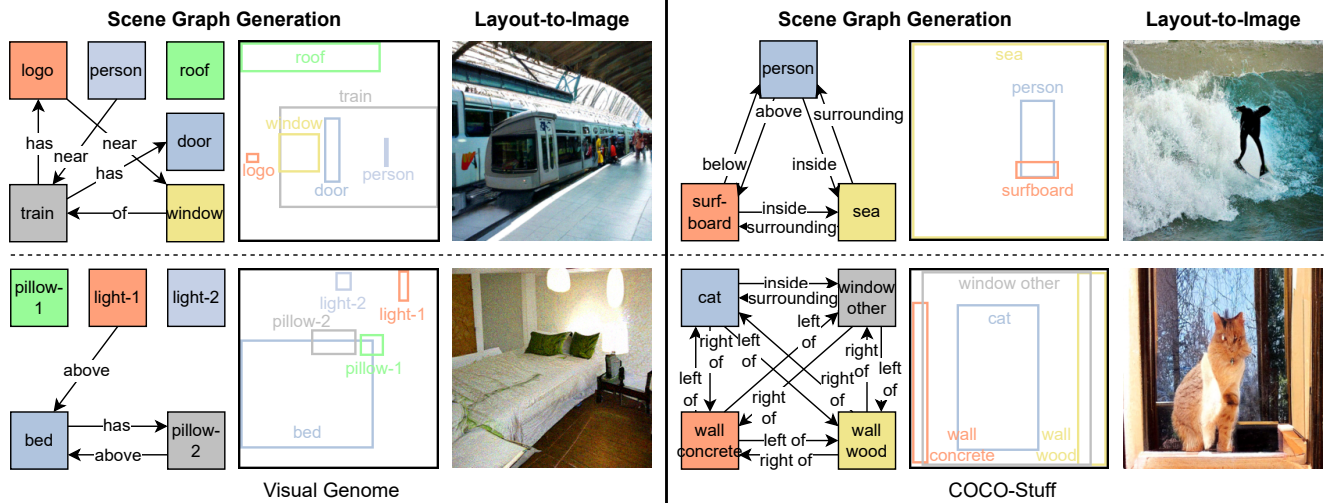


Figure 3. **Qualitative Results.** Scene graphs are generated by DiffuseSG and the corresponding images are produced by [72].

Single Node Completion					
Method	HR@1	HR@10	HR@50	HR@100	mA
DiGress [62]	12.4	21.2	65.3	91.2	20.7
DiffuseSG	13.9	25.7	73.2	94.5	23.6
Single Edge Completion					
Method	HR@1	HR@10	HR@25	HR@50	mA
DiGress [62]	9.8	30.9	41.4	63.2	15.8
DiffuseSG	10.1	35.7	46.2	65.3	19.4

Table 2. **Scene Graph Completion** results on VG validation set.

make it exact K categories. Accuracy is defined as the ratio of the correct predictions (matched to the ground-truth) among the 200 predictions. We then respectively take the average value of HR@K and accuracy over the whole validation set to get the final validation HR@K and mean accuracy (mA) scores. Tab. 2 shows the HR@1/10/50/100 and mA results on the single node completion task. As the results suggested, on all evaluation metrics, our DiffuseSG is consistently better than the DiGress [62] baseline.

Single Edge Label Completion. Similar to the above single node label completion task, we conduct another single edge label completion task, where one edge label is masked out per validation scene graph. The experiment setting and evaluation metrics are the same as the single node label completion setting. For each partially masked scene graph, we predict the edge label 200 times. Tab. 2 shows the mA and HR@1/10/25/50 results. Again, our DiffuseSG is consistently better than DiGress [62] on all evaluation metrics.

Single Bounding Box Completion. Some qualitative examples from DiffuseSG on a single bounding box comple-

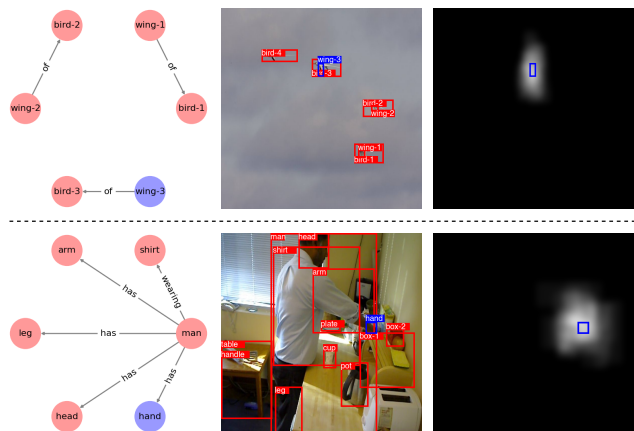


Figure 4. **Single Bounding Box Completion.** The left figure shows the input scene graph, where only the edges and corresponding node labels are shown. The blue node’s bounding box has been masked out. The middle figure shows the untouched (input) bounding boxes with labels in red, the one masked out in blue, along with the corresponding ground-truth image. The right figure shows our generated bounding box heatmap in white along with the target ground-truth bounding box (to be completed) in blue. The heatmap is obtained via generating the bounding box 100 times; the whiter the area, the more overlap at the location.

tion task are shown in Fig. 4, where one bounding box location is masked out given a scene graph, with all other information untouched. The node whose bounding box is masked out has degree at least 1. Note that neither the image nor any image feature is given for the completion task; the image is only for visualization. As seen, DiffuseSG can complete the bounding box in reasonable locations.

Method	VG-5033	COCO-Stuff-3097
BLT [28]	46.36	79.14
LayoutDM [18]	20.82	18.02
DiGress [62]	22.12	20.01
DiffuseSG	<u>21.06</u>	<u>18.33</u>
GT Layouts	17.01	15.61

Table 3. **Layout-to-Image Evaluation.** FID scores are calculated based on the images (in resolution 256×256) generated from a pretrained layout-to-image model [72]. In each column, the best value is **bolded**, and the second best value is underlined.

4.5. Layout-to-Image Evaluation

To evaluate the generated scene graphs / layouts from a perception perspective, we use a pretrained layout-to-image model [72] to generate images based on the generated layouts, and calculate the corresponding FID scores between the generated images and ground-truth ones. We use the evaluation sets used in [72] (*i.e.* VG-5096 and COCO-Stuff-3097). Since there exists a node label set discrepancy between VG-5096 and the VG dataset we used to train our models, we reduce the VG-5096 set to a VG-5033 set; detailed processing procedure is in the Supplemental. For each model on each evaluation set, we only sample one set of layouts (according to the set of node numbers) to generate the images. Tab. 3 shows the results. The last row shows the FID scores for the images generated from the ground-truth (GT) layouts, where the score on VG-5033 is reproduced by us and the one on COCO-Stuff-3097 is borrowed from [72]. DiffuseSG achieves relatively low FID scores compared to other baselines on both sets, and also close to the FID scores calculated from the GT layouts. Though DiffuseSG is slightly worse than LayoutDM, the difference between the FID scores is marginal: only about 0.3, which is visually indistinguishable. Since we are using a pretrained image generation model, this model will actually introduce some generation bias itself: the pretrained model can be good at generating some object categories but not on others. This may cause BLT getting a relatively high FID score on VG-5033. Another reason for why BLT getting high FID scores is that it generates a limited number of node categories. On VG-5033, it generates 119 node categories out of a total of 131; and on COCO-Stuff-3097, it only generates 81 node categories out of a total of 171. This is clearly sub-optimal; in contrast, DiffuseSG covers the full range.

4.6. Scene Graph Detection Evaluation

We take the DiffuseSG trained on VG, and pair it with a trained layout-to-image generation model [72] to form 5,000 scene graph - image pairs, treated as additional training data for a down-stream scene graph detection model. Those additional scene graphs only contain body relations

Data Setting	mR@50/100	R@50/100	Head / Body / Tail
Original	11.9 / 16.0	23.7 / 27.0	26.6 / 19.8 / 9.0
Additional	12.7 / 16.7	23.6 / 26.8	26.4 / 20.7 / 9.7

Table 4. **SGTR Test Results** under the SGDet setting.

as defined in [36]. Detailed process is in the Supplemental.

We use SGTR [37], as an example, to show the value of our generated scene graph - image pairs. We train SGTR under two training data settings: (1) Original, where the training data is the original Visual Genome training data in [37]; (2) Additional, where besides the original training data, we add in our generated 5,000 scene graph - image pairs. Note that these two settings only differ in the training data; both validation and testing data is still the original data for the scene graph detection task. For both data settings, we train SGTR, under the SGDet setting, 4 times and the averaged test results are reported in Tab. 4, where the model for testing is selected via best mR@100 on the validation set. We report results on mean Recalls (mR@50 and mR@100), Recalls (R@50 and R@100), mR@100 on the head, body, and tail partitions (respectively indicated as Head, Body, and Tail in the table).

Comparing our Additional results with the Original results, we can see that our generated scene graph - image pairs do have value, which brings improved results on Body and Tail, and comparable results on Head, which results in increased results on mean Recalls and comparable results on Recalls. As suggested in [60], mean Recall is a better evaluation metric than Recall for the scene graph detection task, because it is less biased to the dominant relation classes. Note that although the generated scene graphs in the additional training data only contain body relations, the Tail results also get improved. This is reasonable, because scene graph is a structure, increasing the confidence of some part of the structural prediction will increase the confidence of other part as well, especially for the tail relations, where the prediction confidence is usually low.

5. Conclusion

In this work, we propose a novel generative task of joint scene graph - image generation. As part of this, we propose DiffuseSG, a diffusion based model for generating scene graphs that adeptly handles mixed discrete and continuous attributes. DiffuseSG demonstrates superior performance on both unconditional scene graph generation and conditional scene graph completion tasks. By pairing DiffuseSG with a conditional image generation model, the joint scene graph - image pair distribution can be obtained. We illustrate the benefits of both DiffuseSG on its own and as part of joint scene graph - image generation. In the future, we are interested in modeling the joint with a single model.

Acknowledgments. This work was funded, in part, by the Vector Institute for AI, Canada CIFAR AI Chairs, NSERC CRC, and NSERC DGs. Resources used in preparing this research were provided, in part, by the Province of Ontario, the Government of Canada through CIFAR, the Digital Research Alliance of Canada alliance.can.ca, companies sponsoring the Vector Institute, and Advanced Research Computing at the University of British Columbia. Additional hardware support was provided by John R. Evans Leaders Fund CFI grant and Compute Canada under the Resource Allocation Competition award.

References

- [1] Diego Martin Arroyo, Janis Postels, and Federico Tombari. Variational transformer networks for layout generation. In *Proceedings of the IEEE/CVF Conference on Computer Vision and Pattern Recognition*, pages 13642–13652, 2021. 2
- [2] Jacob Austin, Daniel D Johnson, Jonathan Ho, Daniel Tarlow, and Rianne Van Den Berg. Structured denoising diffusion models in discrete state-spaces. *Advances in Neural Information Processing Systems*, 34:17981–17993, 2021. 5, 6, 14
- [3] Bashirul Azam Biswas and Qiang Ji. Probabilistic debiasing of scene graphs. In *Proceedings of the IEEE/CVF Conference on Computer Vision and Pattern Recognition*, pages 10429–10438, 2023. 1
- [4] Tim Brooks, Aleksander Holynski, and Alexei A Efros. Instructpix2pix: Learning to follow image editing instructions. In *Proceedings of the IEEE/CVF Conference on Computer Vision and Pattern Recognition*, pages 18392–18402, 2023. 2
- [5] Holger Caesar, Jasper Uijlings, and Vittorio Ferrari. Cocosuff: Thing and stuff classes in context. In *Proceedings of the IEEE conference on computer vision and pattern recognition*, pages 1209–1218, 2018. 5
- [6] Shang Chai, Liansheng Zhuang, and Fengying Yan. Layoutdm: Transformer-based diffusion model for layout generation. In *Proceedings of the IEEE/CVF Conference on Computer Vision and Pattern Recognition*, pages 18349–18358, 2023. 2
- [7] Ting Chen, Ruixiang Zhang, and Geoffrey Hinton. Analog bits: Generating discrete data using diffusion models with self-conditioning. *arXiv preprint arXiv:2208.04202*, 2022. 13, 14
- [8] Vinay Damodaran, Sharanya Chakravarthy, Akshay Kumar, Anjana Umopathy, Teruko Mitamura, Yuta Nakashima, Noa Garcia, and Chenhui Chu. Understanding the role of scene graphs in visual question answering. *arXiv preprint arXiv:2101.05479*, 2021. 1
- [9] Biplab Deka, Zifeng Huang, Chad Franzen, Joshua Hibschman, Daniel Afegan, Yang Li, Jeffrey Nichols, and Ranjitha Kumar. Rico: A mobile app dataset for building data-driven design applications. In *Proceedings of the 30th annual ACM symposium on user interface software and technology*, pages 845–854, 2017. 2
- [10] Bradley Efron. Tweedie’s formula and selection bias. *Journal of the American Statistical Association*, 106(496):1602–1614, 2011. PMID: 22505788. 3
- [11] Patrick Esser, Johnathan Chiu, Parmida Atighehchian, Jonathan Granskog, and Anastasis Germanidis. Structure and content-guided video synthesis with diffusion models. In *Proceedings of the IEEE/CVF International Conference on Computer Vision*, pages 7346–7356, 2023. 2
- [12] Shansan Gong, Mukai Li, Jiangtao Feng, Zhiyong Wu, and LingPeng Kong. Diffuseq: Sequence to sequence text generation with diffusion models. *arXiv preprint arXiv:2210.08933*, 2022. 2
- [13] Kamal Gupta, Justin Lazarow, Alessandro Achille, Larry S Davis, Vijay Mahadevan, and Abhinav Shrivastava. Layout-transformer: Layout generation and completion with self-attention. In *Proceedings of the IEEE/CVF International Conference on Computer Vision*, pages 1004–1014, 2021. 2
- [14] William Harvey, Saeid Naderiparizi, Vaden Masrani, Christian Weilbach, and Frank Wood. Flexible diffusion modeling of long videos. *Advances in Neural Information Processing Systems*, 35:27953–27965, 2022. 2
- [15] Dan Hendrycks and Kevin Gimpel. Gaussian error linear units (gelus). *arXiv preprint arXiv:1606.08415*, 2016. 13
- [16] Jonathan Ho, Ajay Jain, and Pieter Abbeel. Denoising diffusion probabilistic models. In *Advances in Neural Information Processing Systems*, pages 6840–6851. Curran Associates, Inc., 2020. 2, 3, 13, 14
- [17] Mude Hui, Zhizheng Zhang, Xiaoyi Zhang, Wenxuan Xie, Yuwang Wang, and Yan Lu. Unifying layout generation with a decoupled diffusion model. In *Proceedings of the IEEE/CVF Conference on Computer Vision and Pattern Recognition*, pages 1942–1951, 2023. 2
- [18] Naoto Inoue, Kotaro Kikuchi, Edgar Simo-Serra, Mayu Otani, and Kota Yamaguchi. Layoutdm: Discrete diffusion model for controllable layout generation. In *Proceedings of the IEEE/CVF Conference on Computer Vision and Pattern Recognition*, pages 10167–10176, 2023. 2, 5, 6, 8, 14
- [19] John J Irwin, Teague Sterling, Michael M Mysinger, Erin S Bolstad, and Ryan G Coleman. Zinc: a free tool to discover chemistry for biology. *Journal of chemical information and modeling*, 52(7):1757–1768, 2012. 2
- [20] Zhaoyun Jiang, Jiaqi Guo, Shizhao Sun, Huayu Deng, Zhongkai Wu, Vuksan Mijovic, Zijiang James Yang, Jian-Guang Lou, and Dongmei Zhang. Layoutformer++: Conditional graphic layout generation via constraint serialization and decoding space restriction. In *Proceedings of the IEEE/CVF Conference on Computer Vision and Pattern Recognition*, pages 18403–18412, 2023. 2
- [21] Tianlei Jin, Fangtai Guo, Qiwei Meng, Shiqiang Zhu, Xiangming Xi, Wen Wang, Zonghao Mu, and Wei Song. Fast contextual scene graph generation with unbiased context augmentation. In *Proceedings of the IEEE/CVF Conference on Computer Vision and Pattern Recognition*, pages 6302–6311, 2023. 1
- [22] Jaehyeong Jo, Seul Lee, and Sung Ju Hwang. Score-based generative modeling of graphs via the system of stochastic differential equations. In *International Conference on Machine Learning*, pages 10362–10383. PMLR, 2022. 2, 13

- [23] Justin Johnson, Agrim Gupta, and Li Fei-Fei. Image generation from scene graphs. In *Proceedings of the IEEE conference on computer vision and pattern recognition*, pages 1219–1228, 2018. **5**
- [24] Deunsol Jung, Sanghyun Kim, Won Hwa Kim, and Minsu Cho. Devil’s on the edges: Selective quad attention for scene graph generation. In *Proceedings of the IEEE/CVF Conference on Computer Vision and Pattern Recognition*, pages 18664–18674, 2023. **1**
- [25] Akash Abdu Jyothi, Thibaut Durand, Jiawei He, Leonid Sigal, and Greg Mori. Layoutvae: Stochastic scene layout generation from a label set. In *Proceedings of the IEEE/CVF International Conference on Computer Vision*, pages 9895–9904, 2019. **2**
- [26] Tero Karras, Miika Aittala, Timo Aila, and Samuli Laine. Elucidating the design space of diffusion-based generative models. *Advances in Neural Information Processing Systems*, 35:26565–26577, 2022. **3, 13, 14**
- [27] Bahjat Kawar, Shiran Zada, Oran Lang, Omer Tov, Huiwen Chang, Tali Dekel, Inbar Mosseri, and Michal Irani. Imagic: Text-based real image editing with diffusion models. In *Proceedings of the IEEE/CVF Conference on Computer Vision and Pattern Recognition*, pages 6007–6017, 2023. **2**
- [28] Xiang Kong, Lu Jiang, Huiwen Chang, Han Zhang, Yuan Hao, Haifeng Gong, and Irfan Essa. Blt: bidirectional layout transformer for controllable layout generation. In *European Conference on Computer Vision*, pages 474–490. Springer, 2022. **2, 5, 6, 8**
- [29] Ranjay Krishna, Yuke Zhu, Oliver Groth, Justin Johnson, Kenji Hata, Joshua Kravitz, Stephanie Chen, Yannis Kalantidis, Li-Jia Li, David A Shamma, et al. Visual genome: Connecting language and vision using crowdsourced dense image annotations. *International journal of computer vision*, 123:32–73, 2017. **2, 5**
- [30] Alex Krizhevsky, Geoffrey Hinton, et al. Learning multiple layers of features from tiny images. 2009. **14**
- [31] Nupur Kumari, Bingliang Zhang, Richard Zhang, Eli Shechtman, and Jun-Yan Zhu. Multi-concept customization of text-to-image diffusion. In *Proceedings of the IEEE/CVF Conference on Computer Vision and Pattern Recognition*, pages 1931–1941, 2023. **2**
- [32] Sanjoy Kundu and Sathyanarayanan N Aakur. Is-ggt: Iterative scene graph generation with generative transformers. In *Proceedings of the IEEE/CVF Conference on Computer Vision and Pattern Recognition*, pages 6292–6301, 2023. **1**
- [33] Hsin-Ying Lee, Lu Jiang, Irfan Essa, Phuong B Le, Haifeng Gong, Ming-Hsuan Yang, and Weilong Yang. Neural design network: Graphic layout generation with constraints. In *Computer Vision—ECCV 2020: 16th European Conference, Glasgow, UK, August 23–28, 2020, Proceedings, Part III 16*, pages 491–506. Springer, 2020. **2**
- [34] Elad Levi, Eli Brosh, Mykola Mykhailych, and Meir Perez. Dlt: Conditioned layout generation with joint discrete-continuous diffusion layout transformer. *arXiv preprint arXiv:2303.03755*, 2023. **2**
- [35] Jianan Li, Jimei Yang, Aaron Hertzmann, Jianming Zhang, and Tingfa Xu. Layoutgan: Synthesizing graphic layouts with vector-wireframe adversarial networks. *IEEE Transactions on Pattern Analysis and Machine Intelligence*, 43(7): 2388–2399, 2020. **2**
- [36] Rongjie Li, Songyang Zhang, Bo Wan, and Xuming He. Bipartite graph network with adaptive message passing for unbiased scene graph generation. In *Proceedings of the IEEE/CVF Conference on Computer Vision and Pattern Recognition*, pages 11109–11119, 2021. **8, 15**
- [37] Rongjie Li, Songyang Zhang, and Xuming He. Sgtr: End-to-end scene graph generation with transformer. In *proceedings of the IEEE/CVF conference on computer vision and pattern recognition*, pages 19486–19496, 2022. **5, 8, 15**
- [38] Xiang Li, John Thickstun, Ishaan Gulrajani, Percy S Liang, and Tatsunori B Hashimoto. Diffusion-lm improves controllable text generation. *Advances in Neural Information Processing Systems*, 35:4328–4343, 2022. **2**
- [39] Yuheng Li, Haotian Liu, Qingyang Wu, Fangzhou Mu, Jianwei Yang, Jianfeng Gao, Chunyuan Li, and Yong Jae Lee. Gligen: Open-set grounded text-to-image generation. In *Proceedings of the IEEE/CVF Conference on Computer Vision and Pattern Recognition*, pages 22511–22521, 2023. **2**
- [40] Zhenghao Lin, Yeyun Gong, Yelong Shen, Tong Wu, Zhihao Fan, Chen Lin, Nan Duan, and Weizhu Chen. Text generation with diffusion language models: A pre-training approach with continuous paragraph denoise. In *International Conference on Machine Learning*, pages 21051–21064. PMLR, 2023. **2**
- [41] Thomas F Liu, Mark Craft, Jason Situ, Ersin Yumer, Radomir Mech, and Ranjitha Kumar. Learning design semantics for mobile apps. In *Proceedings of the 31st Annual ACM Symposium on User Interface Software and Technology*, pages 569–579, 2018. **2**
- [42] Ze Liu, Yutong Lin, Yue Cao, Han Hu, Yixuan Wei, Zheng Zhang, Stephen Lin, and Baining Guo. Swin transformer: Hierarchical vision transformer using shifted windows. In *Proceedings of the IEEE/CVF international conference on computer vision*, pages 10012–10022, 2021. **4, 13**
- [43] Andreas Lugmayr, Martin Danelljan, Andres Romero, Fisher Yu, Radu Timofte, and Luc Van Gool. Repaint: Inpainting using denoising diffusion probabilistic models. In *Proceedings of the IEEE/CVF Conference on Computer Vision and Pattern Recognition*, pages 11461–11471, 2022. **6**
- [44] Christopher Morris, Martin Ritzert, Matthias Fey, William L. Hamilton, Jan Eric Lenssen, Gaurav Rattan, and Martin Grohe. Weisfeiler and leman go neural: Higher-order graph neural networks. *Proceedings of the AAAI Conference on Artificial Intelligence*, 33(01):4602–4609, 2019. **4**
- [45] Christopher Morris, Yaron Lipman, Haggai Maron, Bastian Rieck, Nils M Kriege, Martin Grohe, Matthias Fey, and Karsten Borgwardt. Weisfeiler and leman go machine learning: The story so far. *arXiv preprint arXiv:2112.09992*, 2021. **4**
- [46] Nithin Gopalakrishnan Nair, Anoop Cherian, Suhas Lohit, Ye Wang, Toshiaki Koike-Akino, Vishal M Patel, and Tim K Marks. Steered diffusion: A generalized framework for plug-and-play conditional image synthesis. In *Proceedings of the IEEE/CVF International Conference on Computer Vision*, pages 20850–20860, 2023. **2**

- [47] Haomiao Ni, Changhao Shi, Kai Li, Sharon X Huang, and Martin Renqiang Min. Conditional image-to-video generation with latent flow diffusion models. In *Proceedings of the IEEE/CVF Conference on Computer Vision and Pattern Recognition*, pages 18444–18455, 2023. [2](#)
- [48] Tianwen Qian, Jingjing Chen, Shaoxiang Chen, Bo Wu, and Yu-Gang Jiang. Scene graph refinement network for visual question answering. *IEEE Transactions on Multimedia*, 2022. [1](#)
- [49] Raghunathan Ramakrishnan, Pavlo O Dral, Matthias Rupp, and O Anatole Von Lilienfeld. Quantum chemistry structures and properties of 134 kilo molecules. *Scientific data*, 1(1): 1–7, 2014. [2](#)
- [50] Hamid Rezaatofighi, Nathan Tsoi, JunYoung Gwak, Amir Sadeghian, Ian Reid, and Silvio Savarese. Generalized intersection over union: A metric and a loss for bounding box regression. In *Proceedings of the IEEE/CVF conference on computer vision and pattern recognition*, pages 658–666, 2019. [4](#)
- [51] Robin Rombach, Andreas Blattmann, Dominik Lorenz, Patrick Esser, and Björn Ommer. High-resolution image synthesis with latent diffusion models. In *Proceedings of the IEEE/CVF conference on computer vision and pattern recognition*, pages 10684–10695, 2022. [2](#)
- [52] Olaf Ronneberger, Philipp Fischer, and Thomas Brox. U-net: Convolutional networks for biomedical image segmentation. In *Medical Image Computing and Computer-Assisted Intervention—MICCAI 2015: 18th International Conference, Munich, Germany, October 5–9, 2015, Proceedings, Part III 18*, pages 234–241. Springer, 2015. [2](#)
- [53] Nataniel Ruiz, Yuanzhen Li, Varun Jampani, Yael Pritch, Michael Rubinstein, and Kfir Aberman. Dreambooth: Fine tuning text-to-image diffusion models for subject-driven generation. In *Proceedings of the IEEE/CVF Conference on Computer Vision and Pattern Recognition*, pages 22500–22510, 2023. [2](#)
- [54] Chitwan Saharia, William Chan, Saurabh Saxena, Lala Li, Jay Whang, Emily L Denton, Kamyar Ghasemipour, Raphael Gontijo Lopes, Burcu Karagol Ayan, Tim Salimans, et al. Photorealistic text-to-image diffusion models with deep language understanding. *Advances in Neural Information Processing Systems*, 35:36479–36494, 2022. [2](#)
- [55] Jascha Sohl-Dickstein, Eric Weiss, Niru Maheswaranathan, and Surya Ganguli. Deep unsupervised learning using nonequilibrium thermodynamics. In *International conference on machine learning*, pages 2256–2265. PMLR, 2015. [2](#)
- [56] Yang Song, Jascha Sohl-Dickstein, Diederik P Kingma, Abhishek Kumar, Stefano Ermon, and Ben Poole. Score-based generative modeling through stochastic differential equations. In *International Conference on Learning Representations*, 2021. [2](#), [3](#), [13](#)
- [57] Wei Sun and Tianfu Wu. Image synthesis from reconfigurable layout and style. In *Proceedings of the IEEE/CVF International Conference on Computer Vision*, pages 10531–10540, 2019. [2](#)
- [58] Wei Sun and Tianfu Wu. Learning layout and style reconfigurable gans for controllable image synthesis. *IEEE transactions on pattern analysis and machine intelligence*, 44(9): 5070–5087, 2021. [2](#)
- [59] Endre Süli and David F. Mayers. *An Introduction to Numerical Analysis*. Cambridge University Press, 2003. [3](#)
- [60] Kaihua Tang, Yulei Niu, Jianqiang Huang, Jiaxin Shi, and Hanwang Zhang. Unbiased scene graph generation from biased training. In *Proceedings of the IEEE/CVF conference on computer vision and pattern recognition*, pages 3716–3725, 2020. [5](#), [8](#)
- [61] Ashish Vaswani, Noam Shazeer, Niki Parmar, Jakob Uszkoreit, Llion Jones, Aidan N Gomez, Łukasz Kaiser, and Illia Polosukhin. Attention is all you need. *Advances in neural information processing systems*, 30, 2017. [2](#)
- [62] Clement Vignac, Igor Krawczuk, Antoine Siraudin, Bohan Wang, Volkan Cevher, and Pascal Frossard. Digress: Discrete denoising diffusion for graph generation. *arXiv preprint arXiv:2209.14734*, 2022. [2](#), [5](#), [6](#), [7](#), [8](#)
- [63] Danfei Xu, Yuke Zhu, Christopher B Choy, and Li Fei-Fei. Scene graph generation by iterative message passing. In *Proceedings of the IEEE conference on computer vision and pattern recognition*, pages 5410–5419, 2017. [5](#)
- [64] Qi Yan, Zhengyang Liang, Yang Song, Renjie Liao, and Lele Wang. Swingnn: Rethinking permutation invariance in diffusion models for graph generation. *arXiv preprint arXiv:2307.01646*, 2023. [2](#)
- [65] Xu Yang, Kaihua Tang, Hanwang Zhang, and Jianfei Cai. Auto-encoding scene graphs for image captioning. In *Proceedings of the IEEE/CVF conference on computer vision and pattern recognition*, pages 10685–10694, 2019. [1](#)
- [66] Sihyun Yu, Kihyuk Sohn, Subin Kim, and Jinwoo Shin. Video probabilistic diffusion models in projected latent space. In *Proceedings of the IEEE/CVF Conference on Computer Vision and Pattern Recognition*, pages 18456–18466, 2023. [2](#)
- [67] Rowan Zellers, Mark Yatskar, Sam Thomson, and Yejin Choi. Neural motifs: Scene graph parsing with global context. In *Proceedings of the IEEE conference on computer vision and pattern recognition*, pages 5831–5840, 2018. [5](#)
- [68] Junyi Zhang, Jiaqi Guo, Shizhao Sun, Jian-Guang Lou, and Dongmei Zhang. Layoutdiffusion: Improving graphic layout generation by discrete diffusion probabilistic models. *arXiv preprint arXiv:2303.11589*, 2023. [2](#)
- [69] Lvmin Zhang, Anyi Rao, and Maneesh Agrawala. Adding conditional control to text-to-image diffusion models. In *Proceedings of the IEEE/CVF International Conference on Computer Vision*, pages 3836–3847, 2023. [2](#)
- [70] Bo Zhao, Lili Meng, Weidong Yin, and Leonid Sigal. Image generation from layout. In *Proceedings of the IEEE/CVF Conference on Computer Vision and Pattern Recognition*, pages 8584–8593, 2019. [2](#)
- [71] Chaofan Zheng, Xinyu Lyu, Lianli Gao, Bo Dai, and Jingkuan Song. Prototype-based embedding network for scene graph generation. In *Proceedings of the IEEE/CVF Conference on Computer Vision and Pattern Recognition*, pages 22783–22792, 2023. [1](#)
- [72] Guangcong Zheng, Xianpan Zhou, Xuwei Li, Zhongang Qi, Ying Shan, and Xi Li. Layoutdiffusion: Controllable diffusion model for layout-to-image generation. In *Proceedings*

of the *IEEE/CVF Conference on Computer Vision and Pattern Recognition*, pages 22490–22499, 2023. [1](#), [2](#), [7](#), [8](#), [15](#)

- [73] Xinru Zheng, Xiaotian Qiao, Ying Cao, and Rynson WH Lau. Content-aware generative modeling of graphic design layouts. *ACM Transactions on Graphics (TOG)*, 38(4):1–15, 2019. [2](#)
- [74] Xu Zhong, Jianbin Tang, and Antonio Jimeno Yepes. Publaynet: largest dataset ever for document layout analysis. In *2019 International Conference on Document Analysis and Recognition (ICDAR)*, pages 1015–1022. IEEE, 2019. [2](#)
- [75] Yiwu Zhong, Liwei Wang, Jianshu Chen, Dong Yu, and Yin Li. Comprehensive image captioning via scene graph decomposition. In *Computer Vision–ECCV 2020: 16th European Conference, Glasgow, UK, August 23–28, 2020, Proceedings, Part XIV 16*, pages 211–229. Springer, 2020. [1](#)

Joint Generative Modeling of Scene Graphs and Images via Diffusion Models

Supplementary Material

6. Implementation Details

6.1. Discrete Input Encodings

Our DiffuseSG utilizes a continuous-state diffusion process. To effectively handle discrete attributes, we implement the following encoding methods.

Scalar. Similar to prior works [16, 22, 26, 56], we map the scalar value to the range $[-1, 1]$. During sampling, we first split the interval $[-1, 1]$ into equal-sized bins in accordance with the number of node or edge categories [22]. We then decode the continuous-valued network output into a discrete label based on the bin into which the output value falls.

Binary-Bit. Following [7], we first convert the integer node/edge attribute into binary bits, and then remap the 0/1 bit values to -1/1 for improved training stability. During sampling, we binarize each value in the network output based on its sign: a positive value is interpreted as 1, and a negative value as 0. We then convert the binary representation back into an integer node or edge label.

One-Hot. We remap the 0/1 values in the one-hot encoding of the original integer node/edge label to -1/1. During sampling, we take the argmax value of the network output to obtain the categorical label.

6.2. DiffuseSG Network Architecture

Our proposed *graph transformer* has two essential components: (1) shifted-window attention mechanism, and (2) downsampling/upsampling layers. In the case of graphs comprising n nodes, their adjacency matrices, incorporating both node and edge attributes, are conceptualized as high-order tensors with $n \times n$ entries. To handle graphs of varying sizes, we standardize the size of these adjacency matrices through padding. Consequently, for different datasets, we accordingly adjust the design parameters to ensure the network is proportionate and suitable for the specific requirements of each dataset.

Shifted-Window Attention. We adopt the shifted window attention technique from [42], which partitions the original grid-like feature map into smaller subregions. Within these subregions, local message passing is executed using self-attention mechanisms. Additionally, the windows are interleavedly shifted, facilitating cross-window message passing, thereby enhancing the overall efficiency and effectiveness of the feature extraction process.

Downsampling/Upsampling Layer. We incorporate channel mixing-based downsampling/upsampling operators to

Hyperparameter	VG	COCO-Stuff
Full tensor size ($n \times n$)	64×64	40×40
Down block attention layers	[1, 1, 3, 1]	[1, 2, 6]
Up block attention layers	[1, 1, 3, 1]	[1, 2, 6]
Number of attention heads	[3, 6, 12, 24]	[3, 6, 12]
Window size	8	10
Token dimension	96	96
Feedforward layer dimension	384	384

Table 5. **Architecture details** of our graph transformer.

effectively diminish or augment the size of the feature map, thereby constructing hierarchical representations. During downsampling, the feature map is divided into four segments based on the parity of the row and column indices, followed by a concatenation process along the channel, which serves to reduce the dimensions of height and width. The upsampling layer performs the inverse operations. It initially splits the tensors along the channel and then reshapes them, effectively reversing the process conducted in the downsampling layer. We also implement one MLP layer right after each downsampling/upsampling layer. In line with the widely recognized U-Net architecture [26, 56], our approach also integrates skip-connections for tensors of identical sizes to enhance the network capacity.

The crucial design parameters of our model are detailed in Tab. 5. It is important to note that within the Down/Up block layers, the initial blocks do not utilize downsampling/upsampling operations. For instance, in the context of the Visual Genome dataset, we effectively implement 3 downsampling layers, which leads to the successive alteration of the feature map dimensions as $64 \rightarrow 32 \rightarrow 16 \rightarrow 8$. In this setup, we opt for a window size of 8, ensuring that the receptive field is sufficiently large to facilitate effective message passing between each pair of nodes. While on COCO-Stuff, we employ 2 downsampling layers, resulting the feature map dimensions as $40 \rightarrow 20 \rightarrow 10$, and thus the window size is set to 10.

MLP Prediction Head. The node/edge attribute MLP prediction head (D_θ^V/D_θ^E) is implemented as two linear layers with a GELU [15] operation injected in between.

6.3. DiffuseSG Diffusion Modeling Details

To ensure the stable training of our diffusion model, we adopt a framework based on the stochastic differential equation (SDE), as proposed in [56]. Additionally, we incorporate a variety of training techniques that have proven effective in image generation contexts: network precondition-

$\sigma_{\min} = 0.002, \sigma_{\max} = 80, \rho = 7$ $S_{\min} = 0.05, S_{\max} = 50, S_{\text{noise}} = 1.003, S_{\text{churn}} = 40, T = 256$ $t_i = (\sigma_{\max}^{\frac{1}{\rho}} + \frac{i}{T-1}(\sigma_{\min}^{\frac{1}{\rho}} - \sigma_{\max}^{\frac{1}{\rho}}))^{\rho}$ $\gamma_i = \mathbf{1}_{S_{\min} \leq t_i \leq S_{\max}} \cdot \min(\frac{S_{\text{churn}}}{T}, \sqrt{2} - 1)$
--

Table 6. **Sampling parameters** in the denoising process.

Algorithm 1 DiffuseSG Sampler.

Require: $D_{\theta}, T, \{t_i\}_{i=0}^T, \{\gamma_i\}_{i=0}^{T-1}$.

- 1: **sample** $\tilde{\mathbf{S}}^{(0)} \sim \mathcal{N}(\mathbf{0}, t_0^2 \mathbf{I}), \hat{\mathbf{S}}_{\text{sc}}^{(0)} = \mathbf{0}$.
 - 2: **for** $i = 0$ to $T - 1$ **do**
 - 3: **sample** $\epsilon \sim \mathcal{N}(\mathbf{0}, S_{\text{noise}}^2 \mathbf{I})$
 - 4: $\hat{t}_i \leftarrow (1 + \gamma_i)t_i$
 - 5: $\tilde{\mathbf{S}}^{(i)} \leftarrow \tilde{\mathbf{S}}^{(i-1)} + \sqrt{\hat{t}_i^2 - t_i^2} \epsilon$
 - 6: $\hat{\mathbf{S}}_{\text{sc}}^{(i)} \leftarrow D_{\theta}(\tilde{\mathbf{S}}^{(i)}, \hat{\mathbf{S}}_{\text{sc}}^{(i-1)}, \hat{t}_i)$
 - 7: $\mathbf{d}_i \leftarrow (\tilde{\mathbf{S}}^{(i)} - \hat{\mathbf{S}}_{\text{sc}}^{(i)}) / \hat{t}_i$
 - 8: $\tilde{\mathbf{S}}^{(i+1)} \leftarrow \tilde{\mathbf{S}}^{(i)} + (t_{i+1} - \hat{t}_i)\mathbf{d}_i$
 - 9: $\hat{\mathbf{S}}_{\text{sc}}^{(i+1)} \leftarrow D_{\theta}(\tilde{\mathbf{S}}^{(i+1)}, \hat{\mathbf{S}}_{\text{sc}}^{(i)}, t_{i+1})$
 - 10: $\mathbf{d}'_i \leftarrow (\tilde{\mathbf{S}}^{(i+1)} - \hat{\mathbf{S}}_{\text{sc}}^{(i+1)}) / t_{i+1}$
 - 11: $\tilde{\mathbf{S}}^{(i+1)} \leftarrow \tilde{\mathbf{S}}^{(i)} + \frac{1}{2}(t_{i+1} - \hat{t}_i)(\mathbf{d}_i + \mathbf{d}'_i)$
 - 12: **end for**
 - 13: **return** $\tilde{\mathbf{S}}^{(T)}$
-

ing [26], self-conditioning [7] and exponential moving average (EMA). For network training, we employ the hyperparameters specified for the ImageNet-64 dataset in [26] for preconditioning purposes; a detailed explanation of these parameters can be found therein. We use Adam optimizer and learning rate being 0.0002. The EMA coefficients used for evaluation are 0.9999 and 0.999 on the Visual Genome and COCO-Stuff datasets respectively.

The pseudocode for our sampling algorithm is presented in Algorithm 1, which follows the stochastic sampler in [26] but with the additional self-conditioning [7] technique. In the algorithm, D_{θ} is the denoising network and $\tilde{\mathbf{S}}^{(t)}$ is the generated scene graph at step t . The associated parameters are detailed in Tab. 6. We opt for $T = 256$ sampling steps to expedite the sampling process, as opposed to the original 1000 steps used in the DDPM framework [16]. In Algorithm 1, with a slight abuse of notations for simplicity, we consider the generated scene graph $(\tilde{\mathbf{S}}, \hat{\mathbf{S}}_{\text{sc}})$, which comprises tuples of node and edge attributes, as a singular tensor, allowing for straightforward addition or subtraction operations. Practically, this is implemented through separate operations on the node and edge tensors.

7. Baseline Details

7.1. LayoutDM during Sampling

For the LayoutDM [18] model, node number can not be specified during sampling. So when evaluating this baseline, we do rejection sampling to form the sample set which has the same node number distribution as the evaluation set. We conduct this process 3 times on the scene graph generation task, and once for the layout-to-image evaluation, to fairly compare LayoutDM with other models.

7.2. D3PM Baseline

Our D3PM [2] baseline is based on the image generation model on the CIFAR-10 dataset [30]. Given a scene graph $\mathbf{S} = (\mathbf{V}, \mathbf{E})^4$ with n nodes, where $\mathbf{V} \in \mathbb{N}^n$ is the node vector containing the scalar node labels and $\mathbf{E} \in \mathbb{N}^{n \times n}$ is the adjacency matrix containing the scalar edge labels, the input to our D3PM baseline is represented as $\mathbf{Q} \in \mathbb{N}^{n \times n \times 3}$, where $\mathbf{Q}_{i,j} = [\mathbf{V}_i, \mathbf{V}_j, \mathbf{E}_{i,j}]$, $\forall i, j \in \{1, 2, \dots, n\}$.

We use two separate discretized Gaussian transition matrices, one for the node category and one for the edge category, to add noise on \mathbf{Q} , resulting in the noised $\hat{\mathbf{Q}}$. We then use a U-Net with two separate prediction heads, each implemented as two convolution layers with a sigmoid operation before each of the convolution layers, to respectively produce the logits of the denoised $\hat{\mathbf{V}}$ and $\hat{\mathbf{E}}$, which then form the logits of the denoised $\hat{\mathbf{Q}}$. We use the $L_{\lambda=0.001}$ (Eq. (5) in [2]), calculated on the logits of $\hat{\mathbf{Q}}$, to train our D3PM baseline. We use Adam optimizer and learning rate being 0.00005 for training. We use $T = 1000$ noising and denoising steps and take the model with EMA coefficient 0.9999 for evaluation.

The β_t (in Eq. (8) in the Appendix of [2]) of the discretized Gaussian transition matrix is increased linearly, for $t \in \{1, 2, \dots, T\}$. On the Visual Genome dataset, We set n to be 64, and β_t is increased linearly from 0.0001 to 0.02 for both node and edge categories. On the COCO-Stuff dataset, n is set to be 36. The β_t is increased linearly from 0.0001 to 0.02 for the node category and from 0.04 to 0.1 for the edge category.

8. Evaluation Details

8.1. Layout-to-Image Evaluation Sets

VG-5033. The original VG-5096 evaluation set has 5096 images, and node (object) numbers between 3 and 30, with a mean of 10.13. Because there exists a node label set discrepancy between the VG-5096 set (178 node categories) and the VG dataset we used to train our scene graph or layout generation models (150 node categories). There are 131

⁴We slightly abuse the notations here, specifically for the D3PM model, compared to the ones in the main text.

node categories in common. On the VG-5096 set, we remove the nodes which are out of the 131 common node labels, and then only keep those layouts whose node numbers are greater than 1. This results in a VG-5033 set which has 5033 layouts, having node numbers between 2 and 28, with a mean of 7.82. We also only use these corresponding 5033 images to calculate the FID. On the VG-5033 set, we guarantee that all node labels generated from all models fall into the common 131 node categories. Following [72], images are sampled once on VG-5033.

COCO-Stuff-3097. The COCO-Stuff-3097 evaluation set has 3097 images, and node numbers between 3 and 8, with a mean of 5.55. COCO-Stuff-3097 and the COCO-Stuff dataset we used for the scene graph generation task share the same node label set, so there is no node number reduction and image removal on COCO-Stuff-3097. Following [72], images are sampled 5 times on COCO-Stuff-3097.

8.2. Generating Additional Training Data for SGTR

We take our DiffuseSG model trained on the Visual Genome dataset, let it generate a set of scene graphs which only contain relations falling into the body partition (as defined in [36]), and then use the pretrained (on VG, with resolution 256×256) layout-to-image generation model [72] to form the scene graph - image pairs. Since there exists some node label set discrepancy between the respective VG annotations used to train the layout-to-image model (178 node categories) and our DiffuseSG model (150 node categories). When forming the scene graph - image pairs, we discard the node whose label is not in the common label set (131 node categories) and its related edges. We randomly choose 5,000 such generated pairs, where node numbers are restricted to be less than 10, as additional training data to train the SGTR [37] model, where the task is given an image, detecting a scene graph (node labels and bounding box locations, and edge labels) from it. We guarantee that for those randomly chosen scene graphs, each of them has at least one edge.

The motivations of why we generating the scene graphs only containing body relations are as follows. First, for the scene graph detection task, there are already many training instances for the head classes, so generating additional head relations may not be beneficial at all. Second, for our scene graph generation task, since the training data for the tail relations is limited, our scene graph generation model may not be able to model the tail class distribution well.

9. More Qualitative Results

9.1. Scene Graph Generation

More qualitative results on the scene graph generation task are shown in Figs. 5 and 6 (Visual Genome) and Figs. 7 and 8 (COCO-Stuff). Scene graphs and the bounding box

locations are generated by DiffuseSG and the corresponding images (in resolution 256×256) are produced by a pretrained layout-to-image model [72]. Note that on the Visual Genome dataset, since there exists some node label set discrepancy between the annotations used to train the layout-to-image model [72] and our DiffuseSG model, we only visualize the scene graphs whose node labels are all in the common node label set (131 node categories).

9.2. Single Bounding Box Completion

More qualitative results of our DiffuseSG on the Visual Genome validation set are shown in Fig. 9. The left figure shows the input scene graph, where only the edges and corresponding node labels are shown. The blue node's bounding box has been masked out. The middle figure shows the untouched (input) bounding boxes with labels in red, the one masked out in blue, along with the corresponding ground-truth image. The right figure shows our generated bounding box heatmap in white along with the target ground-truth bounding box (to be completed) in blue. The heatmap is obtained via generating the bounding box 100 times; the whiter the area, the more overlap at the location. Note that neither the image nor any image feature is given for the completion task; the image is only for visualization.

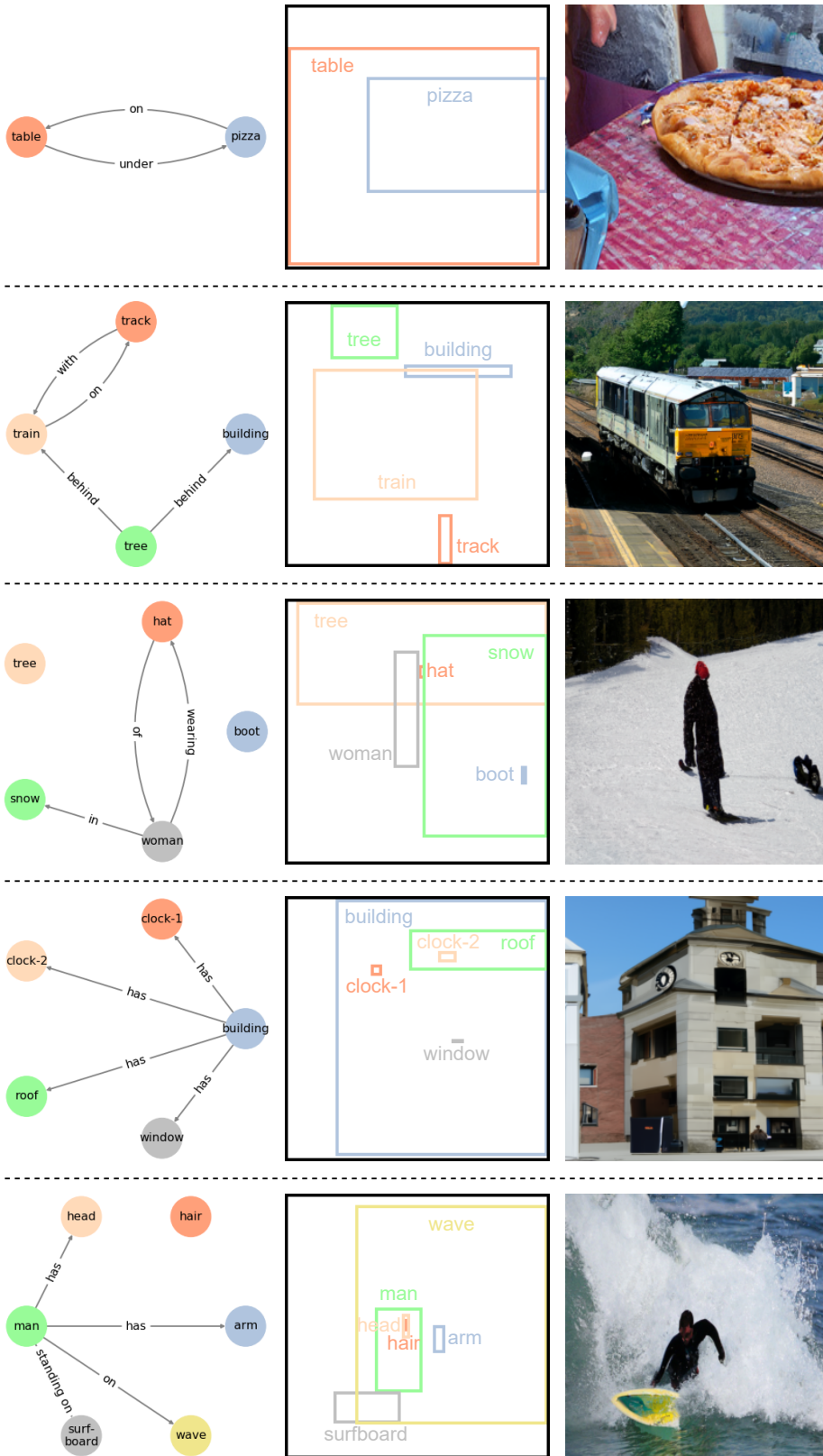


Figure 5. Scene graph generation qualitative results on the Visual Genome dataset.

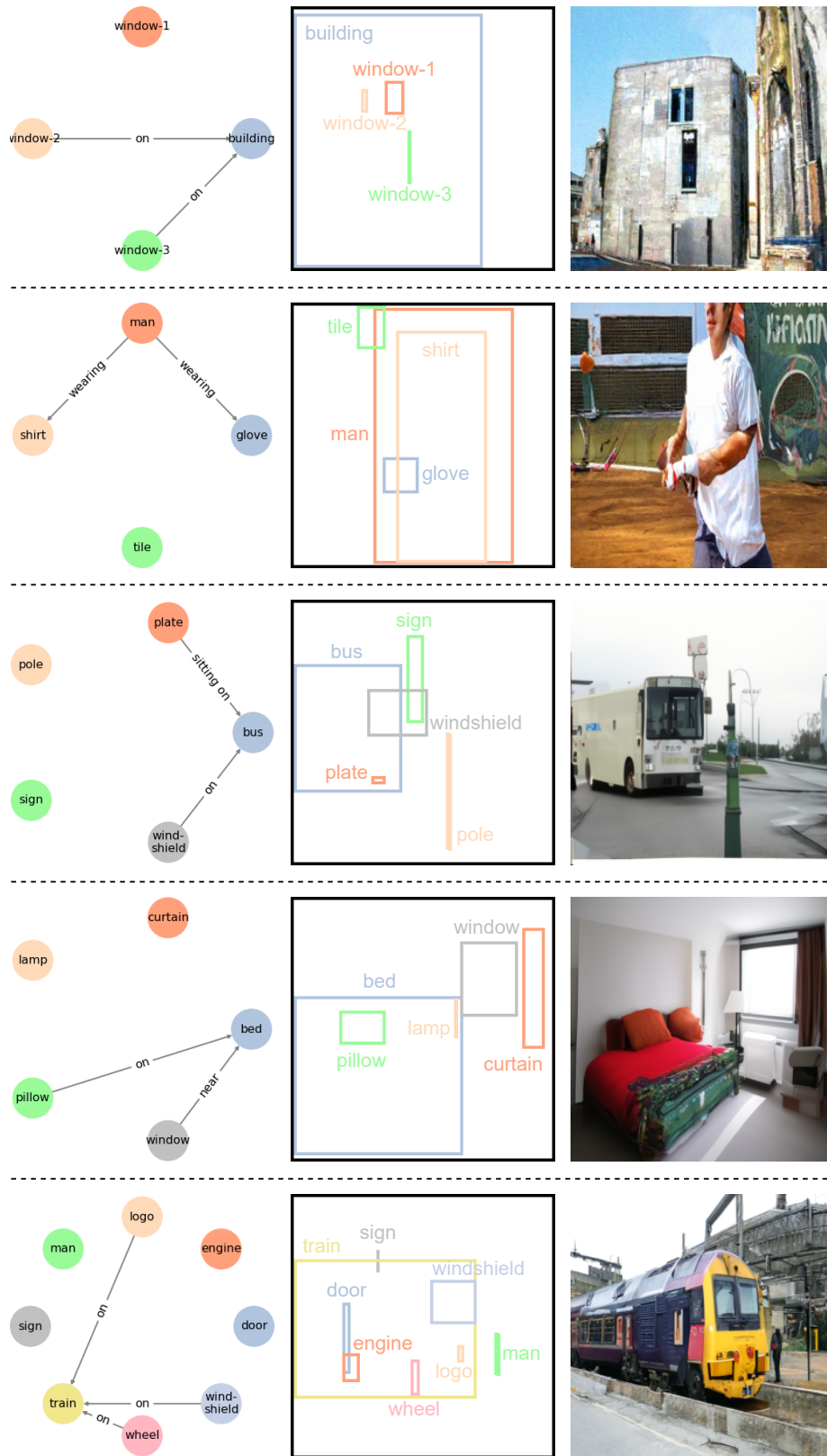


Figure 6. Scene graph generation qualitative results on the Visual Genome dataset.

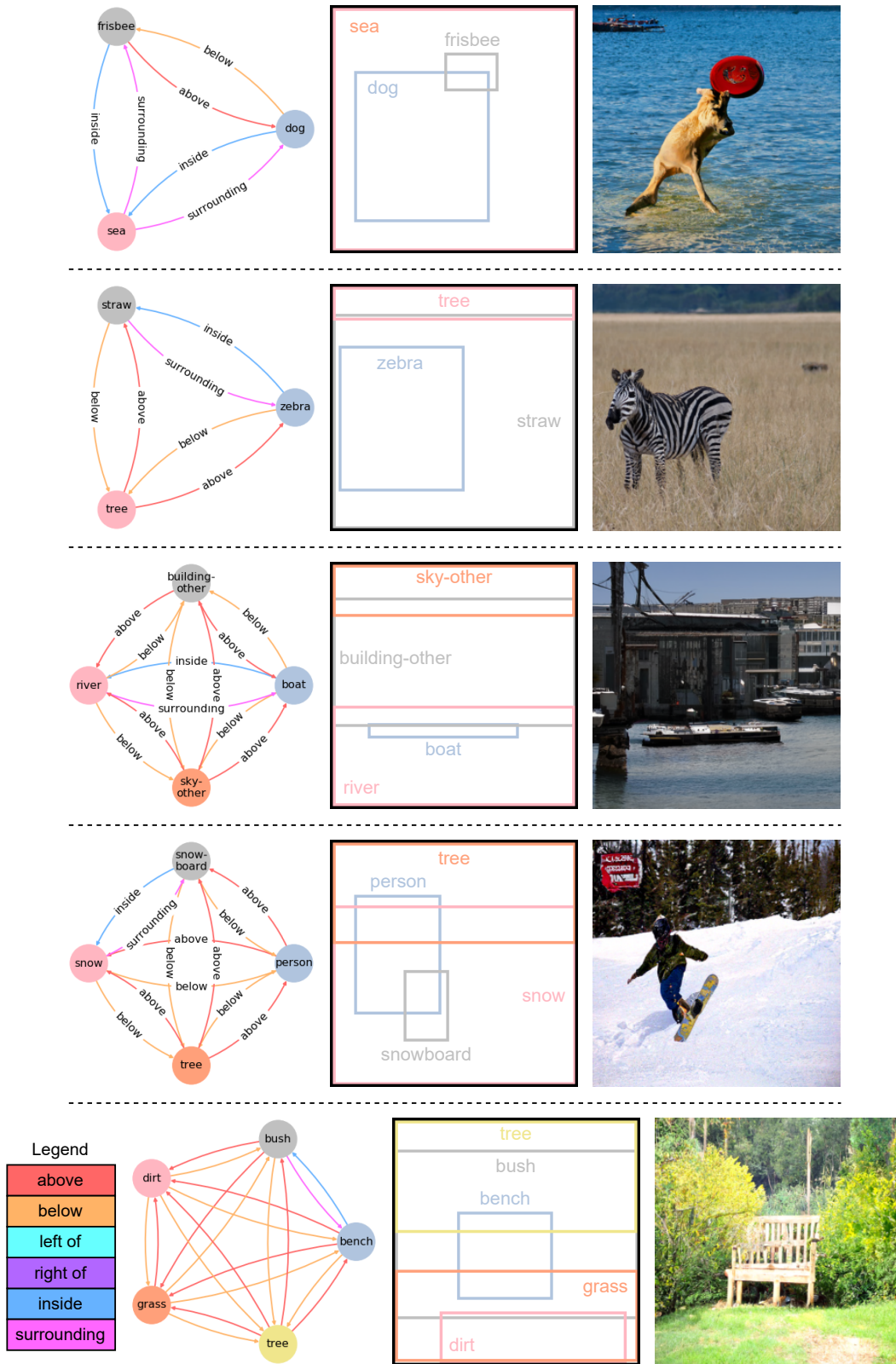


Figure 7. Scene graph generation qualitative results on the COCO-Stuff dataset.

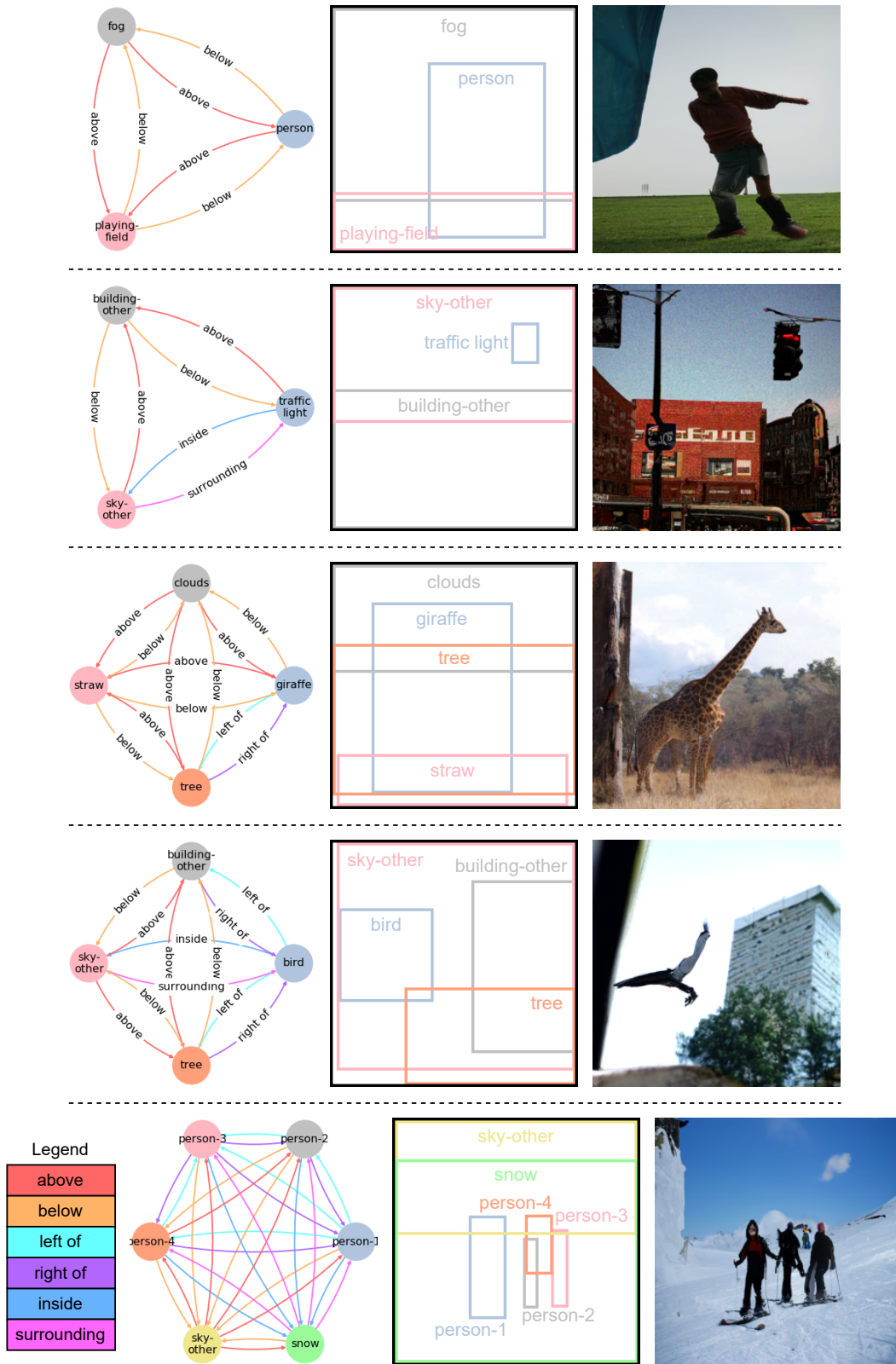


Figure 8. Scene graph generation qualitative results on the COCO-Stuff dataset.

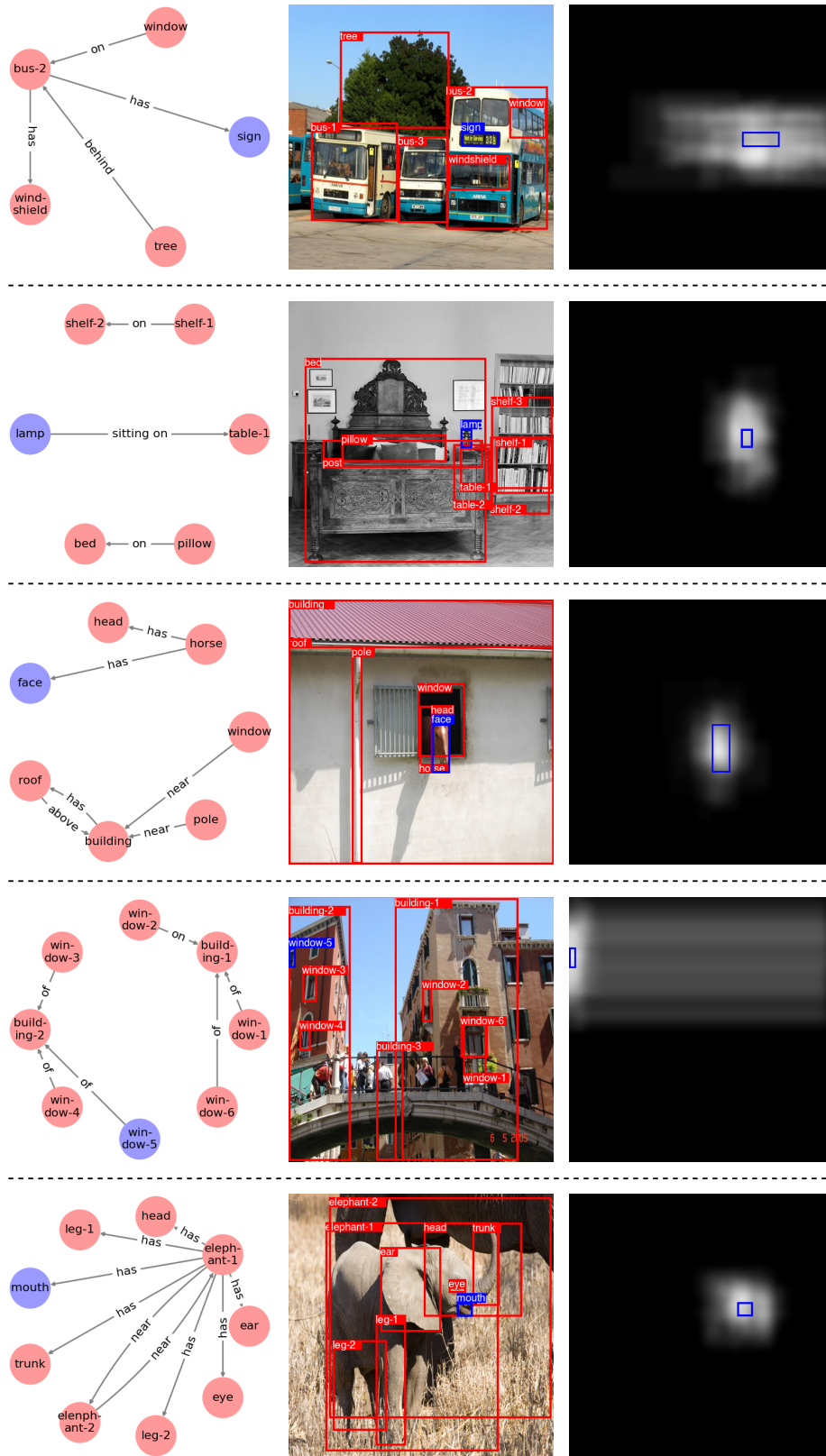


Figure 9. **Single bounding box completion** qualitative results on the Visual Genome validation set.